




# Short-wave infrared light imaging measures tissue moisture and distinguishes superficial from deep burns

Sergey Mironov, PhD<sup>1†</sup>; Charles D. Hwang, BS<sup>2†</sup>; Jean Nemzek, DVM, MS<sup>3</sup>; John Li, MD<sup>2</sup>; Kavitha Ranganathan, MD<sup>2</sup>; Jonathan T. Butts, BS<sup>2</sup>; David J. Cholak, BA<sup>2</sup>; Vladislav A. Dolgachev, PhD<sup>2</sup>; Stewart C. Wang, MD, PhD<sup>2</sup>; Mark Hemmila, MD<sup>2</sup>; Paul S. Cederna, MD, PhD<sup>2</sup>; Michael D. Morris, PhD<sup>4</sup>; Omer Berenfeld, PhD<sup>1†</sup>; Benjamin Levi, MD<sup>2†, #</sup> 

1. Center for Arrhythmia Research, University of Michigan, Ann Arbor, Michigan,
2. Department of Surgery, University of Michigan, Ann Arbor, Michigan,
3. Unit for Laboratory Animal Medicine, University of Michigan, Ann Arbor, Michigan, and
4. Department of Chemistry, University of Michigan, Ann Arbor, Michigan

## Reprint requests:

Benjamin Levi, Burn/Wound and Regenerative Medicine Laboratory, Department of Plastic Surgery, University of Michigan, 1150 W. Medical Center Drive, Ann Arbor, MI, 48109.  
Tel: +734-936-0034;  
Fax: +734-763-6199  
Email: blevi@umich.edu

Manuscript received: September 4, 2019  
Accepted in final form: October 29, 2019

DOI:10.1111/wrr.12779

# Present address: Benjamin Levi, Division of Plastic Surgery, Department of Surgery, University of Michigan Health System, 1500 E Medical Center Drive, SPC 5340, Ann Arbor, MI 48109-5340.

† Equal first authorship.

# Equal senior authorship.

## ABSTRACT

Existing clinical approaches and tools to measure burn tissue destruction are limited resulting in misdiagnosis of injury depth in over 40% of cases. Thus, our objective in this study was to characterize the ability of short-wave infrared (SWIR) imaging to detect moisture levels as a surrogate for tissue viability with resolution to differentiate between burns of various depths. To accomplish our aim, we constructed an imaging system consisting of a broad-band Tungsten light source; 1,200-, 1,650-, 1,940-, and 2,250-nm wavelength filters; and a specialized SWIR camera. We initially used agar slabs to provide a baseline spectrum for SWIR light imaging and demonstrated the differential absorbance at the multiple wavelengths, with 1,940 nm being the highest absorbed wavelength. These spectral bands were then demonstrated to detect levels of moisture in inorganic and in vivo mice models. The multi-wavelength SWIR imaging approach was used to diagnose depth of burns using an in vivo porcine burn model. Healthy and injured skin regions were imaged 72 hours after short (20 seconds) and long (60 seconds) burn application, and biopsies were extracted from those regions for histologic analysis. Burn depth analysis based on collagen coagulation histology confirmed the formation of superficial and deep burns. SWIR multispectral reflectance imaging showed enhanced intensity levels in long burned regions, which correlated with histology and distinguished between superficial and deep burns. This SWIR imaging method represents a novel, real-time method to objectively distinguishing superficial from deep burns.

## INTRODUCTION

Thermal injuries represent a significant public health burden with over 265,000 deaths from burn injuries each year. In the United States alone, over 400,000 people receive medical care for burn injuries annually, with over 10% of these injuries requiring hospitalization and surgical intervention.<sup>1,2</sup>

In the setting of thermal injury, depth of injury dictates therapy and patient outcomes. It is well known that superficial partial-thickness burns heal well without surgery, while deeper, full-thickness injuries require prompt debridement and grafting to prevent the adverse sequelae of scar contractures, infections, and delayed wound healing.<sup>3-5</sup> Thus, the crux of decision making for burn surgeons lies in gauging the necessity of surgical debridement, a determination commonly made within 7 days of presentation.<sup>6</sup> The current standard of care relies on clinical judgment and experience, factors that are difficult to appraise critically due to the

absence of objective data and standardization.<sup>1,2</sup> Additionally, as burn care is provided by both experienced and inexperienced clinicians, objective diagnostic strategies can improve the triage process for patients in the field in a point of care fashion.

Existing modalities for objective preoperative or intraoperative measurements of tissue viability using histology from tissue biopsy are impractical, expensive, invasive, and subject to sampling errors. Additionally, tissue biopsy only provides information at the specific time and site from where the biopsy was taken. Therefore, physical exam is the most commonly utilized method to evaluate depth of injury. Importantly, clinician judgment regarding the need for intervention correlates to objective measures of tissue viability only 60% of the time. Consequently, patients undergo either disproportionately more or less surgery than indicated in approximately 40% of cases leading to longer hospital stays

and poorer outcomes.<sup>1,7,8</sup> Thus, an objective and practical method of measuring the depth of tissue injury has the potential to augment currently available diagnostic modalities.

Methods for better imaging strategies to evaluate tissue viability and guide the need for surgical debridement are necessary and short-wave infrared (SWIR) spectroscopy has been proposed as a potential solution.<sup>9–12</sup> Light in the SWIR spectrum, defined as wavelengths between about 1,000 and 2,500 nm (Figure 1A), contains absorption peaks for O–H bonds (1,430 and 1,940 nm), lipid-associated C–H absorption peaks (1,210, 1,730, and 1,760 nm) and collagen (1,200 and 1,500 nm). Thus, measuring the reflectance of light in the SWIR range was proposed for interrogation of moisture and microscopic structural changes.<sup>12</sup> We further surmise that the SWIR light reflectance sensitivity to tissue factors and moisture could also make it an important marker of skin tissue viability in burns, as suggested by the correlation between water loss and epidermal barrier dysfunction.<sup>13–15</sup> Previous literature, especially in dermatologic journals, has characterized the composition of healthy cutaneous tissues. Namely, strong water signals have been characterized within the stratum corneum and viable epidermis.<sup>13</sup> Furthermore, studies investigating compositional changes after mechanical damage to the cutaneous layer have demonstrated increases in transepidermal water loss, that is, decrease in moisture content.<sup>14,15</sup> Thus, in Figure 1, we illustrate the derived postulate that in viable skin that is well hydrated, increased water content preferentially attenuates the reflectance of the 1,940 nm wavelength compared to the 1,650 or 1,200 nm. However, in full-thickness burns, damage to vasculature and sebaceous glands renders the tissue less hydrated, and it is hypothesized to increase reflectance intensity across the whole SWIR spectrum. Therefore, the goal of the current

study is to evaluate the ability of SWIR imaging to distinguish between burns of different depth. To this end, we applied the SWIR light imaging to inert compounds with variable thicknesses and moisture levels, and ultimately to an in vivo porcine thermal skin injury model.

## METHODS

### Ethical statement

All animal experiments described were approved by the Institutional Animal Care and Use Committee at the University of Michigan, Ann Arbor. This study was carried out in strict accordance with the recommendations in the Guide for the Care and Use of Laboratory Animals of the National Institutes of Health.

### The imaging system and procedures

The SWIR imaging system consisted of three components: (1) a custom-made broadband DC 0.5-kW collimated tungsten-filament light source, (2) filters centered at 1,200, 1,650, 1,940, and 2,250 nm and  $\pm 10$  nm width (Thorlabs, Newton, NJ). The filters were either mounted on a filter wheel attached to the light source or attached to the camera; and (3) a SWIR camera (Xeva-2.35-320, Xenics, Leuven, Belgium) with a Type 2 strained sensor layer sensitive in the 1–2.35  $\mu\text{m}$  wavelengths range. Images of targets were acquired and processed with the software provided with the SWIR camera (Xeneth v2.6, Xenics). Images of  $320 \times 256$  14-bit pixels were collected as 100 frames videos at 15 frames per second with integration time between 12 and

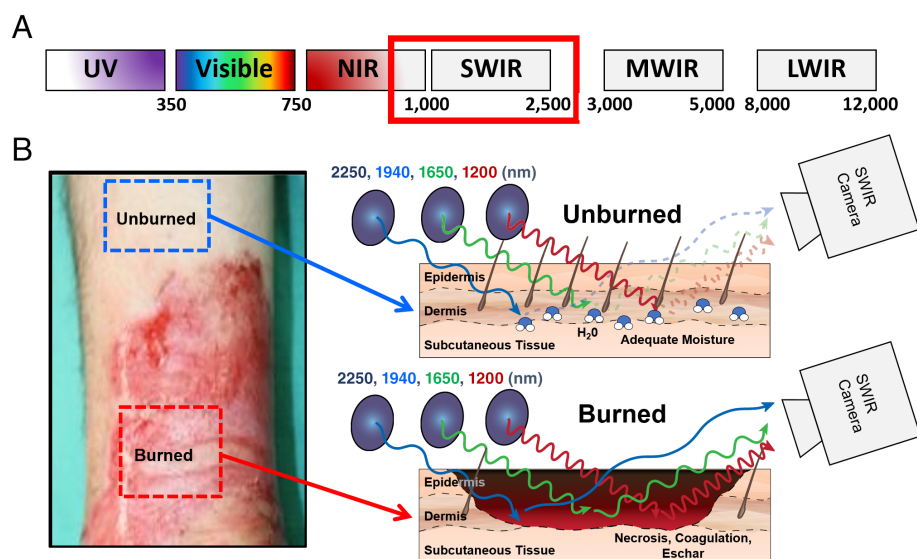


**Figure 1.** SWIR spectrum encompasses excitation frequencies of endogenous cutaneous chromophores. (A) Short-wave infrared (SWIR), defined here between about 1,000 and 2,500 nm, lies in the region between visible–near-infrared (VIS–NIR) and medium-wave infrared (MWIR) encompassing the most specific wavelength marker for water spectroscopy, 1,940 nm. (B) Viable and burned human skin (left) and schematic of SWIR reflectance from these regions (right). In viable skin that is well hydrated (top), increased water content is postulated to preferentially attenuate the reflectance of the 1,940 nm wavelength compared to the 2,250, 1,650, or 1,200 nm. However, in full dermis thickness burns (bottom), damage to vasculature and sebaceous glands renders the tissue less hydrated with proposed increased reflectance intensity across the SWIR spectrum.

30 milliseconds. Camera output yielded pixels intensity values in analog to digital converter units (ADU). Recorded images were processed before analysis with a factory-supplied filter compensating for aberrant pixel values and fixed pattern noise of the imaging sensor. All SWIR readings were conducted in procedures space with controlled temperature (23 °C) and relative humidity (40–50%) in accordance with animal care guidelines.

### Agar preparation for baseline SWIR characteristics

Agar is a heterogeneous mixture of two classes of polysaccharide polymer derived from seaweed and used to cast gel layers in skin phantom model slabs.<sup>16</sup> Baseline SWIR imaging was performed on agar slabs. Slabs using 1 g agar (Sigma Aldrich Corporation, St. Louis, MO) mixed into 30 mL water were constructed in petri dishes (ThermoFisher Scientific, Waltham, MA) as 2D layers with 1, 2, 3, 5, and 10 mm thickness. The petri dishes were then placed in two different configurations for illumination and imaging as schematically described in Figure 2A. In the Epi-illumination (left panel) configuration, the petri dish is illuminated and imaged from the same side such that the light is traversing the slab twice. In the trans-illumination configuration (right panel), the illumination and the imaging are at opposing sides of the slab such that the light is traversing the slab only once. For scaling of absorbance, images were also obtained with empty petri dishes equivalent to zero thickness slabs.

### Baseline moisture models

To ensure that the SWIR imaging system detected variation in moisture levels, we performed three tests. The light source and SWIR camera were placed about 20 cm from the imaged surfaces in an Epi-illumination configuration. A 25-cm diameter P8 grade filter paper (Fisherbrand, Fisher Scientific, Pittsburgh, PA) was applied with 50 µL distilled water at room temperature and imaged at 1,200, 1,650, 1,940, and 2,250 nm simultaneously across the dry and wet regions. Additionally, light reflectance at 1,940 nm, which is a water characteristic O–H bond absorption peak,<sup>17</sup> was imaged from Kimwipe (Kimtech Science Brand; Roswell, Georgia) measuring 4.4 × 8.4 in. sequentially before and after application of 30 µL of distilled water at room temperature. To evaluate the ability of SWIR imaging to detect different levels of moisture in vivo, we also applied no water, 10, 20, and 30 µL of distilled water to the dorsum of three male C57BL/six mice of 6 weeks of age (Charles River, Wilmington, MA). Mice were anesthetized using inhaled 1–3% isoflurane, and euthanized with CO<sub>2</sub> overdose upon completion of the procedure.

### Porcine burn model

The porcine burn model was adapted from the protocol previously described by Singer et al.<sup>18</sup> Five female Yorkshire-cross pigs (Michigan State University Swine Research, East Lansing, MI) weighing 30–35 kg were singly housed with access to water and enrichment and allowed to acclimate to the facilities for at least 7 days prior to the procedures. On the day of a procedure, each pig was sedated with telazol (2.0–8.0 mg/kg IM, Zoetis, Kalamazoo, MI) and xylazine (1.0–3.0 mg/kg IM, AnaSed, Akorn, Decatur, IL). Anesthesia was maintained using 1–4% isoflurane in 100% oxygen delivered by mask. Prior to the burn injury, the pigs were given an intramuscular

injection of 0.05 mg/kg buprenorphine and transdermal buprenorphine patches (total dose of 30 µg/hour, Butrans, Purdue Pharma, Stamford, CT) were applied at the dorsal base of the neck. Animals were euthanized with an overdose of pentobarbital given in the ear vein upon completion of the procedures.

Following anesthesia, the animal's dorsal skin was prepped by chemically removing all hair with Nair for 8–10 minutes followed by a wash with warm water. The skin was then disinfected with three alternating scrubs of chlorhexidine and alcohol, which was allowed to dry. Using a 150 g copper block with an area of 5 × 5 cm<sup>2</sup> and heated in a hot water bath (80 °C) before each application, up to four burns were created by applying the block to the dorsum of the pig for 20 seconds (referred to as short-duration burns) and additional up to four burns deeper burns by applying the heated block for 60 seconds (referred to as long duration burns). The burn regions were 2 cm lateral to the dorsal midline and at least 2 cm apart from one another to ensure independency from the adjacent zone of thermal injury. The burn sites were bandaged with Telfa (Medline, Mundelein, IL) and Tegaderm (3M, St. Paul, MN). Cotton padding was placed over the bandaged burns and the pigs were wrapped loosely with Coban (3M, St. Paul, MN) from thorax to abdomen, then covered with a cotton jacket. Dressings were changed daily using the anesthesia protocol outlined above. Animals were also anesthetized to facilitate image acquisition and punch biopsies for histological analysis.

SWIR imaging of pigs' burns was performed 72 hours after the burns were created. Light source and SWIR camera were set in Epi-illumination configuration affixed to a mobile cart, ensuring a fixed angle of about 30 between optical axes of camera and incident light. Camera was positioned normal to the preparations surface at a distance of about 20 cm. Each burn site was imaged individually along with two flanking control regions from an unburned area of nearby skin. SWIR images of reflectance from a template uniform background (Figure 2) were used as a normalizing reference for the distribution of illumination intensity in space. Areas of 50 × 50 pixels (~5 × 5 mm<sup>2</sup>) at the center of each region of interest, excluding burn edges and biopsy sites, were used to determine average intensity values.

### Histological analysis

Full burn thickness punch biopsies (4 mm diameter) were acquired at the time of anesthesia from the porcine skin. The tissue specimens were fixed in 10% buffered formalin for 24 hours at 4 °C and dehydrated in serial preparations of ethanol. In order to accurately assess the depth of the burns, specimens were embedded in paraffin (Leica EG1150 C, Leica, Wetzlar, Germany) and sectioned into 5-µm-thick longitudinal slices (Leica RM2255, Leica). Sections were then deparaffinized, rehydrated, and stained with hematoxylin & eosin (H&E) and Picrosirius red.<sup>19</sup> Analysis for burn depth was primarily based on collagen alteration depth as determined by hyaline changes and seroproteinaceous infiltrate.<sup>20,21</sup> Depth of injury was determined within specimens by measuring the length from the outer edge of the epidermis layer to the level of the deepest area of collagen coagulation. All images were manually segmented in FIJI/ImageJ to circumscribe the entire region of the burn and calculate average depth. Segmentations were performed by three blinded analyzers previously trained by a board certified clinical pathologist's practice set.

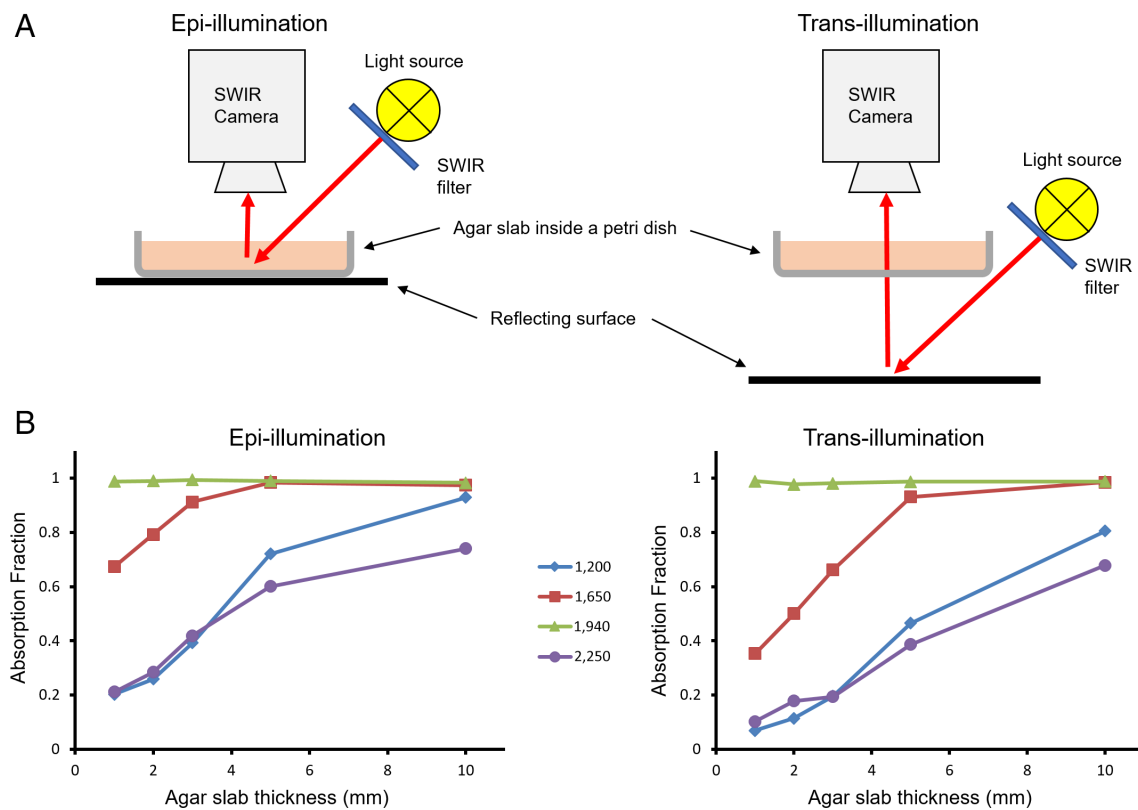


**Figure 2.** Basic short-wave infrared (SWIR) imaging characteristics. (A) Imaging setups. In Epi-illumination configuration (left) the light source and the camera are on the same side of specimen and the light transverses twice the agar slab. In the Trans-illumination configuration, the light transverses only once the agar slab. In both configurations, the light intensity at the camera depends on absorbance and scattering of the light along its path; however, air–agar surface scattering does not depend on the agar slab thickness. (B) Absorption fraction vs. agar slab thicknesses for 1,200, 1,659, 1,940, and 2,250-nm light. Apart from light at 1940 nm which is fully absorbed by slabs 1 mm or more thick, the absorbance of other wavelengths is greater in the Epi-illumination (left) than in the Trans-illumination (right) configuration, but is sensitive to the slab thickness at least up to 5 mm thick.

### Statistical analysis

Animal imaging and histology data are confirmed to be normally distributed with Shapiro–Wilk test and are reported as mean  $\pm$  standard deviations, except where noted. One-sided or two-sided student's *t* tests were used to show significant difference between imaged and histology groups, respectively. Weighted linear regression analysis was performed on moisture imaging. Levene's (homoscedasticity) test was applied to porcine histology analysis. Two-way analysis of variance (ANOVA) was applied to porcine spectral imaging of burns of various durations. For each test, *p* value less than 0.05 is considered significant.

## RESULTS

### Basic SWIR light imaging characteristics

For basic characterization of SWIR light absorption and reflection in a biological phantom model, we performed a well-controlled Epi- and Trans-illumination imaging experiments on agar slices of variable thicknesses.<sup>16</sup> Figure 2A shows the imaging setups (see "Methods" section) and Figure 2B describes the dependence of

the absorbance fraction on the thickness of the agar slabs. The absorbance fraction was calculated as the space averaged ratio of intensity without agar minus the intensity with agar to the intensity without agar. The absorption fraction graphs show approximately similar relative dependency for Epi- and Trans-illumination imaging for all wavelengths. It is seen that the 1,200-, 1,650-, and 2,250-nm light is gradually and monotonically more absorbed by slabs with increasing thicknesses between 1 and 5 mm regardless of the Epi- and Trans-illumination settings. The data also show that for both illumination configurations our light sources and camera system is not capable to determine the agar slab thickness by the 1,940-nm light because that light is almost entirely absorbed already by a 1-mm thickness slab. The information from this test suggests that the 1,650-nm light is absorbed in agar more than 1,200- and 2,250-nm light. It is also suggested that the 1,940-nm light should be used mainly for submillimeter surface-most skin layer analyses and that the 1,200- and 2,250-nm light could be used for deeper skin layers analyses.

### SWIR light imaging delineates moisture content

A baseline demonstration of water effect on SWIR reflectance is demonstrated in Figure 3A. White paper was wetted with 50  $\mu$ L distilled water and then the dry and wetted

regions were imaged with the Xeva-2.35-320 camera under collimated tungsten Epi-illumination at 1,200-, 1,650-, 1,940-, and 2,250-nm light. Images (top) show a central dark spot corresponding to the wet region. A profile of light intensity across the dry and wet regions (red line) demonstrates that the relative reflectance of the moist regions in this setup was less than the surrounding dry regions. Notably the reflectance at 1,940 nm was the lowest among all four wavelengths at 50% in the wetted relative to the dry regions. Following, the effect of water on reflectance was quantified at the 1,940 nm sequentially in the same region before and after application of 30  $\mu\text{L}$  of water. Reflectance intensity wavelength was significantly less in the wet region compared to dry region with a mean difference between dry and wet regions of the paper measuring 635 ADU ( $p < 0.0001$ ; Figure 3A,B). Taken together, Figure 3A,B demonstrate that regional water application is detectable using our SWIR, mainly 1,940 nm, Epi-illumination imaging approach. Similar differences between moist and dry tissue were noted when varying degrees of water were applied topically to the dorsum of a mouse (Figure 3C). In this model, there was a significant decrease in spectral intensity in moist skin compared to

dry skin after application of 10, 20, and 30  $\mu\text{L}$  water. Cumulative data from three mice shown in Figure 3D demonstrates a monotonic decreased in averaged 1,940-nm reflectance intensity with increasing amounts of applied water (in ADU):  $794 \pm 83$ ,  $444 \pm 73$ ,  $334 \pm 90$ , and  $235 \pm 43$  for 0, 10, 20, and 30  $\mu\text{L}$  water, respectively ( $p < 0.05$  between all groups comparisons). A weighted linear regression analysis of the data in Figure 3D yielded  $R = 0.953$  (adjusted  $R^2 = 0.863$  and  $p = 0.047$ ) and confirmed that light reflectance at 1,940 nm is sensitive to water content.<sup>12</sup>

### SWIR light imaging and depth of damaged tissue in a porcine burn model

Next, we used a clinically relevant porcine model to study spectral SWIR light reflectance in deep and superficial burns. Figure 4A shows a total of eight burn regions in a sample animal: in each animal, up to four short (S) and four long (L) duration contact with a heated metal block were applied in the demarcated dorsal regions with unburned surrounding area. At 48 hours postburn, biopsies from the

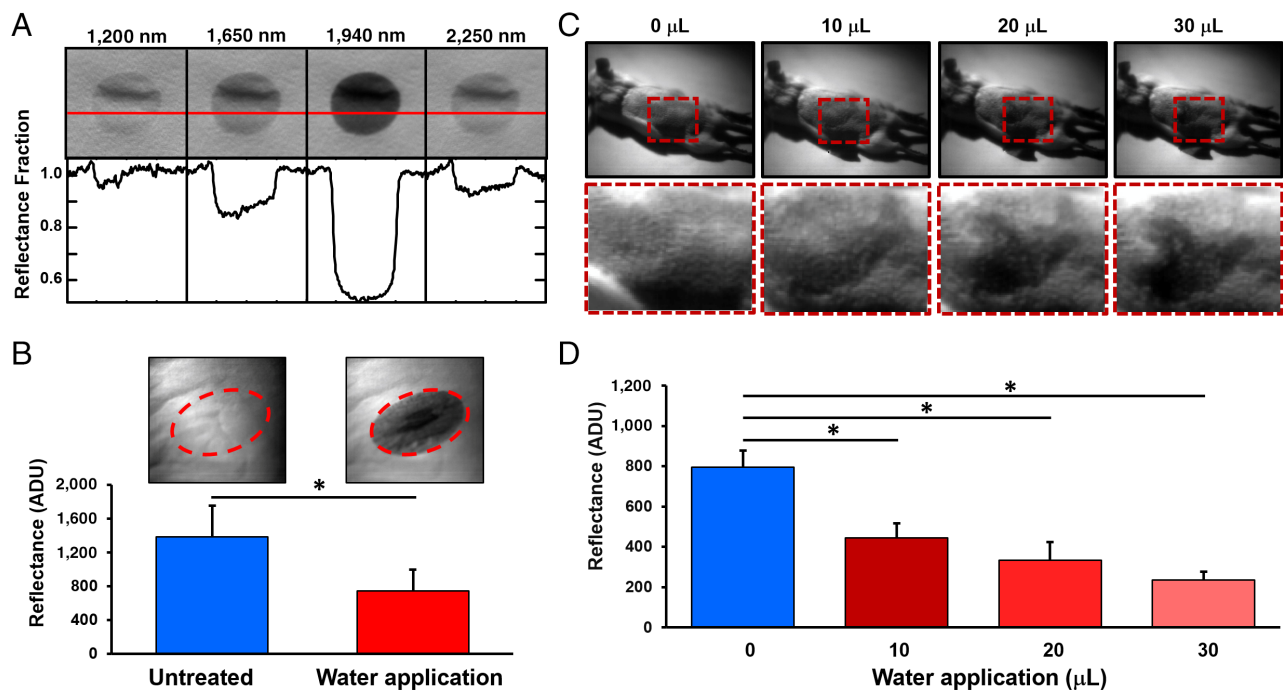


**Figure 3.** Short-wave infrared (SWIR) light reflectance detects moisture levels in biologic tissue. (A) As baseline, 50  $\mu\text{L}$  distilled water was applied on four inert substrate surfaces (P8 Grade filter paper, Fisher Scientific) and imaged with the Xeva-2.35-320 camera under collimated tungsten Epi-illumination at 1,200-, 1,650-, 1,940-, and 2,250-nm light. Top: Reflectance images normalized to no substrate reflectance show attenuated reflectance in wetted regions at center for all wavelengths. Dark bands in wetted regions result from wrinkles. Bottom: Reflectance normalized to dry regions along red line in images. Reflectance fraction is visibly least attenuated for 1,200 nm and most attenuated at 1940 nm (about 50% of dry regions). (B) An inert substrate (Kimwipe) was imaged with the 1940-nm filter on the camera under tungsten Epi-illumination before and after application of 30  $\mu\text{L}$  water. Significant signal attenuation is present within the wetted region demarcated by red dashed line. SWIR reflectance at 1940 nm demonstrates diminished reflectance after water application ( $1,382 \pm 369$  vs.  $747 \pm 249$  ADU,  $p < 0.0001$ ). (C) SWIR reflectance images at 1940 nm of mouse skin under normal conditions and after administration of 10, 20, and 30  $\mu\text{L}$  of water, demonstrating progressive decrements of signal reflectance with increasing water administration. (D) SWIR reflectance at 1940 nm demonstrating diminished signal of dry depilated dorsum of mouse at progressive administrations of 10, 20, and 30  $\mu\text{L}$  of water ( $794 \pm 83$  vs.  $444 \pm 73$ ,  $334 \pm 90$ ,  $235 \pm 43$  ADU,  $p < 0.001$ ).  $N = 3$  mice/group.  $p < 0.05$  demarcated by asterisk.

burned regions were excised and at 72 hours postburn, the burn and unburned regions were imaged with the spectral SWIR. Figure 4B shows four unprocessed SWIR images from sample short (top) and long (bottom) duration burn regions. The images demonstrate heterogeneous reflectance with heterogeneous demarcation of the short (pink arrow) and long (red arrow) heat application regions and whereby overall reflectance intensity at 1,200 and 2,250 nm is visibly higher than at 1,650 and 1,940 nm. In Figure 4C, the unprocessed images of Figure 4B were processed to differentiate between the short and long duration burn regions. The processing consisted of summing the 1,650 and 2,250 nm images and normalization by the 1,940-nm image to account for nonuniform illumination. The resulted images show pixels in the short burn (top)

are darker than in the long burn (middle), which is further illustrated by an image of the difference in their pixels values (L-S, bottom) showing more white pixels in the burned regions and black pixels in the surrounding area.

To quantify the general ability of the SWIR imaging to distinguish between burn regions, we processed a total of  $n = 17$  short and  $n = 17$  long duration heated regions, along with nearby unburned regions, imaged at the four separated wavelengths. The processing of the images for reflectance fraction of each individual region and wavelength included normalizing the images with the corresponding spectral images of reflectance from a reference surface to account for the nonuniform illumination (see “Methods” section). The cumulative reflectance fractions for all the regions and all

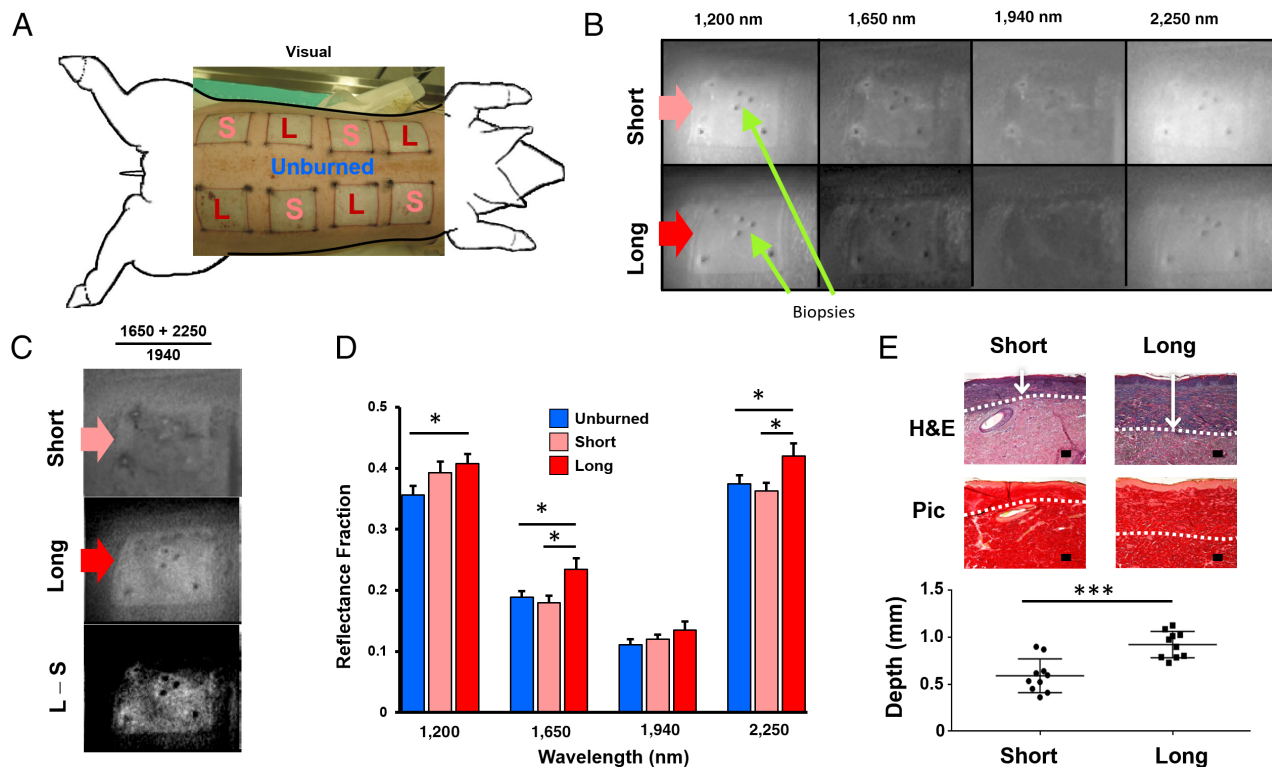


**Figure 4.** SWIR reflectance can delineate superficial and deep burns in a porcine burn model: (A) In a porcine thermal injury model, a heated block delivered heat in 5 × 5-cm regions for short (S) and long (L) durations. Picture illustrates eight regions in a sample animal under ambient visual light imaging. Unburned regions in between burns were used as controls. (B) SWIR images from sample animal with long (top) and short (bottom) duration heated regions with surrounding unburned areas. The heated regions (pink and red arrows) and sample biopsies regions (green arrows) are indicated. (C) Images showing processing outcomes for short (top) and long (middle) burns images whereby images from B at 1,650 and 2,250 nm were summed and then divided by the corresponding 1,940 nm images. The higher brightness in the long vs. short burn areas is corroborated by a bright area in the difference image (L-S, bottom). Difference is reduced in the top of the heated regions where skin surface is far from normal to the optical axis. (D) Collective analysis of SWIR images taken for each burn site ( $N = 5$  pigs,  $n = 17$  regions/group). Graph shows mean ± standard error of SWIR reflectance fraction of intensity of unburned (blue), short (pink) and long (red) burn regions, respectively, at: 1200 nm ( $0.3562 \pm 0.0146$ ,  $0.3925 \pm 0.0187$ ,  $0.4079 \pm 0.0155$ ), 1,650 nm ( $0.1884 \pm 0.0102$ ,  $0.18 \pm 0.011$ ,  $0.2347 \pm 0.0179$ ), 1,940 nm ( $0.111 \pm 0.0089$ ,  $0.12 \pm 0.0074$ ,  $0.1348 \pm 0.0145$ ), and 2,250 nm ( $0.3741 \pm 0.0146$ ,  $0.363 \pm 0.13$ ,  $0.42 \pm 0.0204$ ). Asterisks indicate  $p < 0.05$ . (E) Sample micrographs of biopsy sections from short and long burn regions (top) and cumulative analysis (bottom). White-dotted lines on standard H&E stained micrographs demarcate burned vs. normal dermis. White-dotted lines on Picrosirius (Pic) red stains corroborated burn boundaries by highlighting changes to collagen ultrastructure. White arrows = depth from epidermis. Scale bars = 100  $\mu$ m. Manual segmentations by three blinded analyzers averaged each individual specimen and show short burn resulted in burn depth of  $590 \pm 57 \mu$ m vs. a long burn resulted in burn depth of  $922 \pm 72 \mu$ m ( $p = 0.0002$ , triple asterisks).  $N = 5$  pigs,  $n = 10$  specimen/group.

wavelengths are shown in Figure 4D. A two-way ANOVA analysis on the data from the five animals reveals that reflected fraction is different for both each wavelength ( $p < 0.001$ ) and for each treatment (i.e., unburned, short- and long-duration heating,  $p = 0.011$ ). As shown in the graph, imaged wavelengths of 1,200, 1,650, and 2,250, but not 1,940 nm, show a significant 10–20% higher averaged reflectance in the long-duration burn in comparison with the unburned region. The insensitivity of the 1,940-nm reflectance to the burns is consistent with the insensitivity of that wavelength to agar thickness shown in Figure 2B. Notably, the 1,650- and 2,250-nm reflectance intensity from long-duration heating regions was 10–20% higher while the 1,940-nm reflectance is not significantly different from the short-duration heating regions, which explains the processing of images at those wavelengths to distinguish between the sample short and long burns illustrated in Figure 4C.

In addition to the SWIR imaging, biopsies were taken from the edges and center of the burned regions for histology analysis as shown in Figure 4B (green arrows). Figure 4E shows sample H&E and Picrosirius red stained sections from short (left) and long (right) burns duration biopsies. The superimposed outlined edges of collagen alteration<sup>20,21</sup> used as a marker for burn depth corroborates the deeper dermis incurred damage in tissue under heating. The graph in Figure 4E analyzes 10 sampled biopsies in each treatment region and finds that on average the long-duration heating damages tissue as deep as  $922 \pm 45 \mu\text{m}$  while the short-duration heating damages tissue as  $590 \pm 57 \mu\text{m}$  deep ( $p < 0.001$ ). Taken together, the data presented in Figure 4 show that we have generated a deep and superficial dermis burned regions in the porcine model and that SWIR imaging at specific wavelengths of 1,650 and 2,250 nm can distinguish between these two regions.

## DISCUSSION

Our study aimed at demonstrating the conceptual utility of SWIR (~1,000–2,500 nm) imaging in diagnosing the depth of viable tissue in skin burns. We have demonstrated that specific wavelengths of the SWIR light range are sensitive to tissue moisture in mice and distinguish between superficial and deep burn injury in porcine.

### Models of skin burns

Papp et al.<sup>21</sup> previously validated a reproducible model of pig burn for histological analysis of burn depth. While the authors were able to demonstrate reliability and reproducibility of their model, their deeper burns all converged to a deep burn depth. In order to produce a more tunable model, we performed our inductive burns with cooler blocks and for longer contact times (20 °C cooler, and  $\times 2$ –4 longer, respectively). Meyerholz et al.<sup>20</sup> previously characterized parameters to determine burn depth via histology in an acute rat model, demonstrating a linear relation between contact time and average depth. Although their study's biopsies were performed at 5 hours, extrapolating their dose-dependency linear regression on burn depth is consistent with our porcine model that remained stable to the day 3 time point (not shown). This resolution affords advantages in the validation of separate diagnostic modalities and characterization of treatment effects in a

burned skin model that more closely resembles human tissues.

### SWIR light and imaging of biological tissue

The benefit of imaging skin burns in the SWIR spectrum lies in the ability of light in this range to penetrate tissue deeper than light in the visible and near-infrared (NIR) spectrum, while limiting penetration to avoid confounding deep tissue edema, as occurs in mid-infrared light. Additionally, the presence of resonance wavelengths for O–H and C–O vibrational overtone in this region of the SWIR light detects compounds such as collagen, lipid, and water with greater sensitivity than NIR imaging or other modalities. Moisture levels, a tissue quality commonly evaluated by burn surgeons to gauge the depth of tissue injury, are best captured in the SWIR spectrum, with signal absorbance at 1,940 nm that is 260-fold greater than at 970 nm in the NIR spectrum.<sup>22</sup> While non-spectral modalities have also been proposed, variability in skin conditions and imaging methods hamper comparisons of water absorbance of SWIR light between different studies.<sup>23</sup> Furthermore, the need for a consistent electrical contact with the skin surface as well as an exquisite sensitivity to ambient temperature render electrical measurements for the assessment of trans-epidermal water loss, such as capacitance, as sub-optimal when compared to our imaging results.<sup>13,15</sup>

In this study, we demonstrate that SWIR imaging at certain wavelengths detects differences in moisture and differentiates superficial from deep burns in a noninvasive fashion using an in vivo porcine model with histology as the gold standard for comparison. These distinctions, while binary and not yet representative of the clinical spectrum of burn depths encountered, suggest a future role for SWIR imaging in determining viability of tissue in the acute setting. The moisture imaging data shown in Figure 3 is consistent with the ability of 1,940 nm reflectance to detect moisture levels in vivo amounts of  $< 30 \mu\text{L}$ , but the relation of 1,940-nm light reflectance to burn depth has not been fully established as our imaging analysis in the agar slabs of  $> 1 \text{ mm}$  in thickness (Figure 2) and burns with damaged collagen at depth between about 0.5 and 1 mm (Figure 4) show similar levels of absorbance or reflectance of 1,940-nm light. Further investigation is required to clarify the effect of water content at different skin depths on the SWIR light reflectance.<sup>13–15</sup>

Our two-way ANOVA of the burns images demonstrated that the SWIR reflectance depends on both the wavelengths of the images and the burn depths. In general, the combined analysis of reflectance-sensitive wavelengths could enhance the burn depth discrimination, while a reflectance that is indifferent to the physiological underlying conditions of the substrate could be used for calibration purposes. Accordingly, in this study we utilized sample burns images captured at 1,940 nm, who showed no significant reflectance sensitivity to the skin conditions (Figure 4D), to normalize the images captured at 1,650 and 2,250 nm. As illustrated in Figure 4C, the panels of the normalized images augmented the visual impact of the images in Figure 4B, who showed a modest 10–20% reflectance differences (Figure 4D), and enabled a clearer distinction between the unburned, the short and the long burn regions. Future research following the concepts utilized here may identify other SWIR wavelengths and processing for a better analysis of different burn depths.

Our results agree with those of previous studies that indicate the benefit of SWIR technology. SWIR optical sensing of skin has been previously used to characterize porcine and human skin.<sup>12,24,25</sup> However, these measurements have been performed *ex vivo*, with a limited SWIR range and have not been used to assess burns or traumatic wounds. SWIR has also been used to identify atherosclerotic plaque and stages of malignancy in breast cancer.<sup>26,27</sup> The noninvasive method of measuring the composition and nature of deeper anatomic structures is critically important to the overarching benefit of SWIR imaging. SWIR imaging is currently used to quantify skin moisture after application of topical facial cosmetics<sup>11,12</sup>; however, SWIR imaging has not been tested in the past with regards to its efficacy in the setting of thermal injury.

### Clinical management of burns

The current standard of care for thermal injury is debridement to viable tissue layers; however, the precise plane of transition is difficult to determine across an injury and under or over debridement ultimately lead to increased patient morbidity.<sup>1,7,8</sup> We propose that use of our noninvasive point of care SWIR imaging modality will allow clinicians to more clearly diagnose superficial vs. deep burns based on surface moisture and tissue viability as the key variables of interest guiding the treatment toward excision or non-surgical management. This modality, like a conventional visible light point and shoot camera, does not contact the patient and does not require the injection of fluorescent markers.<sup>22</sup> Given short, efficient acquisition times, the development of a novel, accurate, noncontact, rapid, and portable point of care technology for use in military, veteran, and civilian patients will allow for a more objective assessment of burn wound depth.

Although technologies have been developed to facilitate burn injuries management including determination of viability, currently available modalities, including laser Doppler imaging (LDI), indocyanine green (ICG) video angiography, and NIR imaging, have important limitations that have restricted the potential for standardized clinical use in military, veteran, and civilian populations.<sup>22</sup> While new technologies have recently come forth to define burn depth, these modalities have important limitations that restrict their potential for standardized clinical use.<sup>28</sup> LDI measures the volumetric flux of blood at a site to determine tissue viability. While studies have demonstrated greater than 95% correlation between histology and LDI in terms of accuracy of determining tissue viability, this method requires large instrumentation that is not portable and can be very expensive. Most importantly, however, LDI is only able to be used within the narrow window of 2–5 days after injury, and is not recommended for use in patients with comorbidities such as anemia, cellulitis, or vascular disease.<sup>29,30</sup> Thus, clinical applicability is severely limited as a result of these restrictions. ICG videoangiography is another modality of macroimaging used to visualize the patency of vasculature within the deep dermis. Using this system, patients receive an intravenous injection of ICG. Tissues that are viable demonstrate high uptake of ICG, while tissues that are less viable demonstrate lower uptake visualized as lower fluorescence. The main limitation of this modality is the need for intravascular injection, an invasive procedure that is difficult to repeat and can result in pain, anaphylaxis, headache, and urticaria.<sup>29</sup> Another example of a technology that has demonstrated limited clinical adoption is NIR imaging. Although this device visualizes burn wound edema as a metric of tissue injury, the particular wavelength used is only able to

evaluate the quality of deeper tissues and not the more superficial tissues that require debridement.<sup>9,22,31</sup> Furthermore, NIR is not able to reliably and reproducibly evaluate surface moisture, which is the primary region of interest with our new system. Finally, both NIR and LDI depend on blood flow; thus, burn debridement performed on extremities under tourniquet precludes use of these technologies.

### Limitations

There are important limitations to consider. First, our analysis is a proof of concept validation of the feasibility of SWIR imaging in determining the extent of burn injury, but it is not yet correlated to differences in clinical outcomes. Second, our study was conducted in only two burn depths and we do not have sufficient spatial resolution in biopsies for histological data to support the fine spatial details that represent all pathological conditions that may affect light reflectance. Furthermore, our burn study was performed at 72 hours postinjury and did not perform long-term follow-up of burned specimens and debridement based on the SWIR readings. Finally, although the porcine thermal injury model has been extensively validated, intrinsic differences to human skin necessitate additional studies to assess the efficacy of SWIR systems in human patients.<sup>32</sup>

### CONCLUSIONS

Objective measures of burn wound depth are important to properly diagnose and treat patients with burns. Our study in mice and porcine models suggests that SWIR imaging can detect skin moisture and can distinguish between superficial and deep burns under certain conditions. Thus SWIR imaging and metrics may represent a new noninvasive technology to guide tissue debridement. Once validated in humans, SWIR technology will add objective data to supplement pre-existing clinical standards of care.

### ACKNOWLEDGMENTS

The authors would like to thank the staff at the University of Michigan Microscopy and Imaging Laboratory (MIL) for their assistance.

### SOURCE OF FUNDING

This study was supported in part by the Coulter Translational Research Partnership Program at the University of Michigan (BL, OB), NIH/National Institute of General Medical Sciences Grant K08GM109105-0, NIH R01GM123069, ACS Clowes Award, Department of Defense W81XWH-18-2-0038 (BL), Department of Defense/US Army W81XWH-16-1-0574 (JN), NIH/National Heart, Lung, and Blood Institute R01-HL118304 (SM, OB), and Research Grants from Medtronic, Inc., and Abbott (SM, OB).

### CONFLICT OF INTEREST

OB: in portions of time during the performance of this study he was a cofounder and Scientific Officer of Rhythm Solutions, Inc., Research and Development Director for S.A.S. Volta Medical and consultant to Acutus Medical and also received Honoraria from Aurora Medical, Biosence-Webster and Boston Scientific. None of these activities is related to the present study.



## REFERENCES

- Sen CK, Gordillo GM, Roy S, Kirsner R, Lambert L, Hunt TK, et al. Human skin wounds: a major and snowballing threat to public health and the economy. *Wound Repair Regen* 2009; 17: 763–71.
- Kauvar DS, Wolf SE, Wade CE, Cancio LC, Renz EM, Holcomb JB. Burns sustained in combat explosions in Operations Iraqi and Enduring Freedom (OIF/OEF explosion burns). *Burns* 2006; 32: 853–7.
- D'Avignon LC, Chung KK, Saffle JR, Renz EM, Cancio LC, Prevention of Combat-Related Infections Guidelines Panel. Prevention of infections associated with combat-related burn injuries. *J Trauma* 2011; 71: S282–9.
- Hospenthal DR, Murray CK, Andersen RC, Bell RB, Calhoun JH, Cancio LC, et al. Executive summary: guidelines for the prevention of infections associated with combat-related injuries: 2011 update: endorsed by the Infectious Diseases Society of America and the Surgical Infection Society. *J Trauma* 2011; 71: S202–9.
- Levi B, Jayakumar P, Giladi A, Jupiter JB, Ring DC, Kowalske K, et al. Risk factors for the development of heterotopic ossification in seriously burned adults: a National Institute on Disability, Independent Living and Rehabilitation Research burn model system database analysis. *J Trauma Acute Care Surg* 2015; 79: 870–6.
- Saffle JR. Critical care management of the severely burned patient. In: Parrillo JE, editor *Critical care medicine*, 4th ed. Saunders, Philadelphia, PA, 2014; 1177–98.
- Loder S, Peterson JR, Agarwal S, Eboda O, Brownley C, DeLaRosa S, et al. Wound healing after thermal injury is improved by fat and adipose-derived stem cell isografts. *J Burn Care Res* 2015; 36: 70–6.
- Heimbach D, Engrav L, Grube B, Marvin J. Burn depth: a review. *World J Surg* 1992; 16: 10–5.
- Cross KM, Leonardi L, Payette JR, et al. Clinical utilization of near-infrared spectroscopy devices for burn depth assessment. *Wound Repair Regen* 2007; 15: 332–40.
- Edgar DW, Briffa NK, Cole J, Tan MH, Khoo B, Goh J, et al. Measurement of acute edema shifts in human burn survivors—the reliability and sensitivity of bioimpedance spectroscopy as an objective clinical measure. *J Burn Care Res* 2009; 30: 818–23.
- Egawa M, Yanai M, Maruyama N, Fukaya Y, Hirao T. Visualization of water distribution in the facial epidermal layers of skin using high-sensitivity near-infrared (NIR) imaging. *Appl Spectrosc* 2015; 69: 481–7.
- Arimoto H, Egawa M. Imaging wavelength and light penetration depth for water content distribution measurement of skin. *Skin Res Technol* 2015; 21: 94–100.
- Ezerskaia A, Uzunbajakava NE, Puppels GJ, de Sterke J, Caspers PJ, Urbach HP, et al. Potential of short-wave infrared spectroscopy for quantitative depth profiling of stratum corneum lipids and water in dermatology. *Biomed Opt Express* 2018; 9: 2436–50.
- Vergou T, Schanzer S, Richter H, Pels R, Thiede G, Patzelt A, et al. Comparison between TEWL and laser scanning microscopy measurements for the in vivo characterization of the human epidermal barrier. *J Biophotonics* 2012; 5: 152–8.
- Rosado C, Rodrigues LM. In vivo study of the physiological impact of stratum corneum sampling methods. *Int J Cosmet Sci* 2003; 25: 37–44.
- Chen AI, Balter ML, Chen MI, Gross D, Alam SK, Maguire TJ, et al. Multilayered tissue mimicking skin and vessel phantoms with tunable mechanical, optical, and acoustic properties. *Med Phys* 2016; 43: 3117–31.
- Ali JH, Wang WB, Zevallos M, Alfano RR. Near infrared spectroscopy and imaging to probe differences in water content in normal and cancer human prostate tissues. *Technol Cancer Res Treat* 2004; 3: 491–7.
- Singer AJ, Hirth D, McClain SA, Crawford L, Lin F, Clark RA. Validation of a vertical progression porcine burn model. *J Burn Care Res* 2011; 32: 638–46.
- Chvapil M, Speer DP, Owen JA, Chvapil TA. Identification of the depth of burn injury by collagen stainability. *Plast Reconstr Surg* 1984; 73: 438–41.
- Meyerholz DK, Piester TL, Sokolich JC, Zamba GK, Light TD. Morphological parameters for assessment of burn severity in an acute burn injury rat model. *Int J Exp Pathol* 2009; 90: 26–33.
- Papp A, Kiraly K, Harma M, Lahtinen T, Uusaro A, Alhava E. The progression of burn depth in experimental burns: a histological and methodological study. *Burns* 2004; 30: 684–90.
- Wilson RH, Nadeau KP, Jaworski FB, Tromberg BJ, Durkin AJ. Review of short-wave infrared spectroscopy and imaging methods for biological tissue characterization. *J Biomed Opt* 2015; 20: 030901.
- Bashkatov AN, Genina EA, Kochubey VI, Tuchin VV. Optical properties of human skin, subcutaneous and mucous tissues in the wavelength range from 400 to 2000 nm. *J Phys D Appl Phys* 2005; 38: 2543–55.
- Zamora-Rojas E, Aernouts B, Garrido-Varo A, Saeys W, Pérez-Marín D, Guerrero-Ginel JE. Optical properties of pig skin epidermis and dermis estimated with double integrating spheres measurements. *Innovative Food Sci Emerg Technol* 2013; 20: 343–9. <https://doi.org/10.1016/j.ifset.2013.06.008>
- Edgar MP, Gibson GM, Bowman RW, Sun B, Radwell N, Mitchell KJ, et al. Simultaneous real-time visible and infrared video with single-pixel detectors. *Sci Rep* 2015; 5: 10669.
- Cerussi A, Shah N, Hsiang D, Durkin A, Butler J, Tromberg BJ. In vivo absorption, scattering, and physiologic properties of 58 malignant breast tumors determined by broadband diffuse optical spectroscopy. *J Biomed Opt* 2006; 11: 044005.
- Wang J, Geng YJ, Guo B, Klima T, Lal BN, Willerson JT, et al. Near-infrared spectroscopic characterization of human advanced atherosclerotic plaques. *J Am Coll Cardiol* 2002; 39: 1305–13.
- Heimbach DM, Afromowitz MA, Engrav LH, Marvin JA, Perry B. Burn depth estimation—man or machine. *J Trauma* 1984; 24: 373–8.
- Devgan L, Bhat S, Aylward S, Spence RJ. Modalities for the assessment of burn wound depth. *J Burns Wounds* 2006; 5: e2.
- Hoeksema H, Van de Sijpe K, Tondt T, Hamdi M, Van Landuyt K, Blondeel P, et al. Accuracy of early burn depth assessment by laser Doppler imaging on different days post burn. *Burns* 2009; 35: 36–45.
- Cross KM, Leonardi L, Gomez M, Freisen JR, Levasseur MA, Schattka BJ, et al. Noninvasive measurement of edema in partial thickness burn wounds. *J Burn Care Res* 2009; 30: 807–17.
- Sullivan TP, Eaglstein WH, Davis SC, Mertz P. The pig as a model for human wound healing. *Wound Repair Regen* 2001; 9: 66–76.